Algorithm Theoretical Basis Document (ATBD) for GSICS Infrared Inter-Calibration of Imagers on MTSAT-1R/-2 and Himawari-8/-9 using AIRS and IASI Hyperspectral Observations

Masaya Takahashi

Meteorological Satellite Center

Japan Meteorological Agency

Version: 2017-12-19 (v1.1)

Document Change Record

Version	Date	Author / changed by	Summary of Changes
v0.1	2010-07-14	Hiromi Owada	・ First version for MTSAT-1R and -2 based on a template prepared by GSICS Research and Data Working Group.
v1.0	2017-08-10	Masaya Takahashi	・ Added Himawari-8 and -9 AHI infrared inter-calibration. ・ Changed section 6.b (Smooth Results) to 6.b and c (Calculate Coefficients for GSICS Near-Real-Time and Re-Analysis Correction).
v1.1	2017-12-19	Masaya Takahashi	・ Updated Himawari-8 AHI thresholds in 4.a.iv.

Contents

0. Introduction

The Global Space-based Inter-Calibration System (GSICS) aims to inter-calibrate a diverse range of satellite instruments to produce corrections ensuring their data are consistent, allowing them to be used to produce globally homogeneous products for environmental monitoring. Although these instruments operate on different technologies for different applications, their inter-calibration can be based on common principles: Observations are collocated, transformed, compared and analysed to produce calibration correction functions, transforming the observations to common references. To ensure the maximum consistency and traceability, it is desirable to base all the inter-calibration algorithms on common principles, following a hierarchical approach, described here.

This algorithm is defined as a series of generic *steps* revised at the GSICS Research and Data Working Group web meeting (December 2009):

1) Subsetting
2) Collocating
3) Transforming
4) Filtering
5) Monitoring
6) Correcting

Each step comprises a number of discrete components, outlined in the Contents.

Each component can be defined in a hierarchical way, starting from purposes, which apply to all inter-calibrations, building up to implementation details for specific instrument pairs:

i. Describe the purpose of each component in this generic data flow.
ii. Provide different options for how these may be implemented in general.
iii. Recommend procedures for the inter-calibration class (e.g. GEO-LEO).
iv. Provide specific details for each instrument pair (e.g. AHI-IASI).

Each component is defined independently and may exist in different versions. The implementation of the algorithm need only follow the overall logic – so the components need not be executed strictly sequentially. For example, some parts may be performed iteratively, or multiple components may be combined within a single loop in the code.

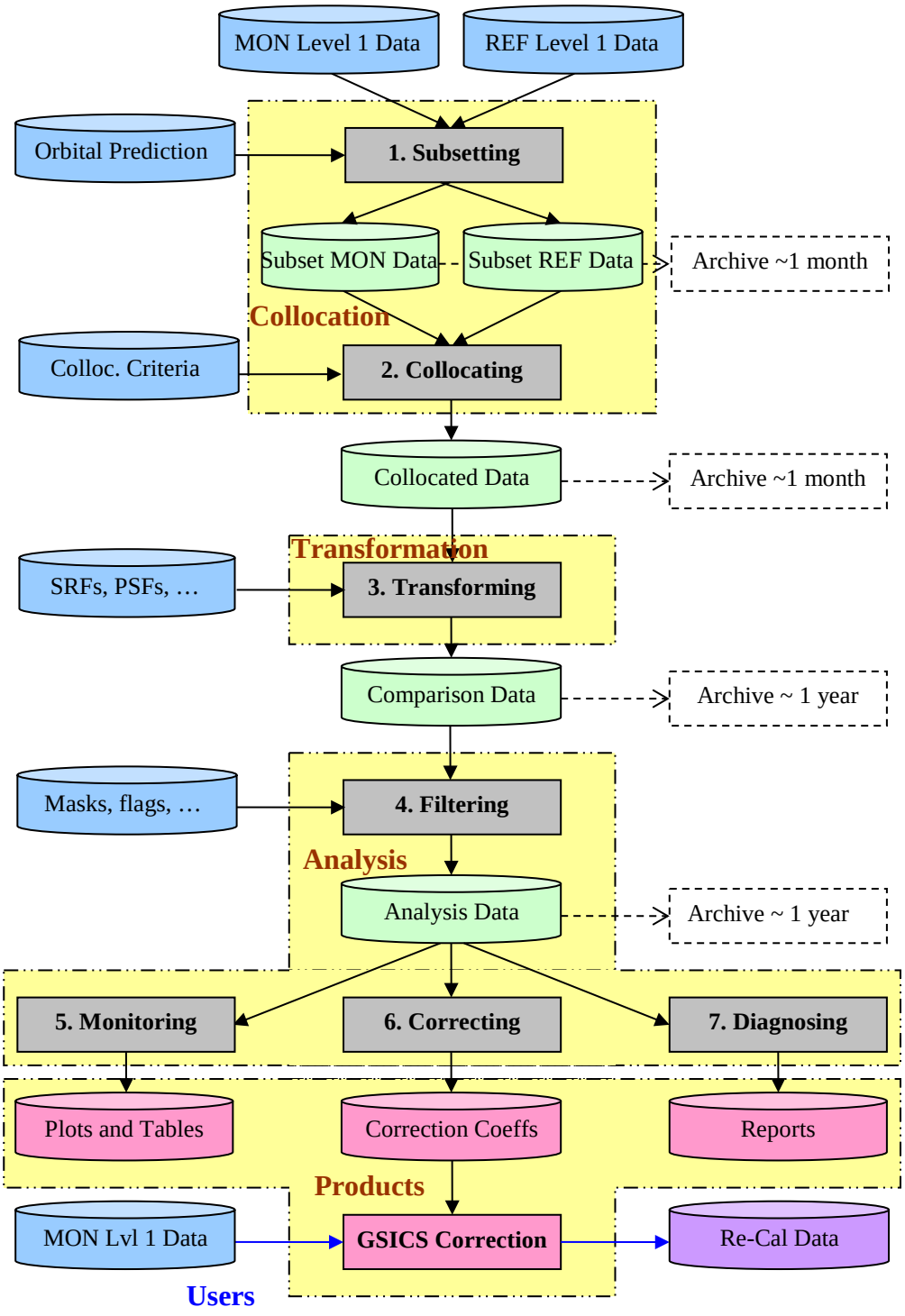

Figure 1: Diagram of generic data flow for inter-calibration of monitored (MON) instrument with respect to reference (REF) instrument

0.1 JMA's MTSAT/Himawari-AIRS/IASI Inter-calibration Algorithm

This document forms the Algorithm Theoretical Basis Document (ATBD) for the inter-calibration of the infrared channels of Japanese Advanced Meteorological Imager (JAMI) on the Geostationary (GEO) Multi-functional Transport Satellite (MTSAT)-1R, Imager on MTSAT-2 and Advanced Himawari Imager (AHI) on Himawari-8 and -9 satellites with the Atmospheric Infrared Sounder (AIRS) on board Low-Earth Orbiting (LEO) Aqua satellite or with the Infrared Atmospheric Sounding Interferometer (IASI) on board LEO Metop satellites. Infrared channel configurations for GEO imagers of MTSAT and Himawari series are shown in Table 1.

Table 1: Infrared channel configuration of AHIs on Himawari-8/-9, Imager on MTSAT-2 and JAMI on MTSAT-1R. Wlen is the central wavelength [μm], and Sres represents spatial resolution at the Sub Satellite Point [km].

MTSAT-1R/JAMI	Name	IR4	IR3					IR1		IR2	
	Wlen	3.78	6.75					10.82		12.02	
	Sres	4	4					4		4	
MTSAT-2/Imager	Name	IR4	IR3					IR1		IR2	
	Wlen	3.74	6.78					10.81		12.02	
	Sres	4	4					4		4	
Himawari-8/AHI	Name	B07	B08	B09	B10	B11	B12	B13	B14	B15	B16
	Wlen	3.89	6.24	6.94	7.35	8.59	9.64	10.41	11.24	12.38	13.28
	Sres	2	2	2	2	2	2	2	2	2	2
Himawari-9/AHI	Name	B07	B08	B09	B10	B11	B12	B13	B14	B15	B16
	Wlen	3.83	6.25	6.96	7.34	8.59	9.63	10.41	11.21	12.36	13.31
	Sres	2	2	2	2	2	2	2	2	2	2

This document includes different versions of each component of the MTSAT/Himawari-AIRS/IASI specific algorithm. The prototype developed at JMA was implemented for MTSAT-1R/JAMI inter-calibration in July 2008. The updated one for MTSAT-2/Imager, Himawari-8/AHI and Himawari-9/AHI inter-calibration was introduced in July 2010, March 2015 and February 2017, respectively. The product version is defined in the *processing_leve*l Global Attribute of the product's netCDF file.

As for the instrument's name of MTSAT series, both MTSAT-1R and MTSAT-2 have the same specific images. However, MTSAT-1R's imager was named "JAMI" (Japanese Advanced Meteorological Imager) and MTSAT-2's one was named "Imager" because the makers of imager are different. In this document, "MTSAT" is used in the descriptions of specifics on both MTSAT imagers except when the instrument's name should be cleared.

1. **Subsetting**

Acquisition of raw satellite data is obviously a critical first step in an inter-calibration method based on comparing collocated observations. To facilitate the acquisition of data for the purpose of inter-comparison of satellite instruments, prediction of the time and location of collocation events is also important.

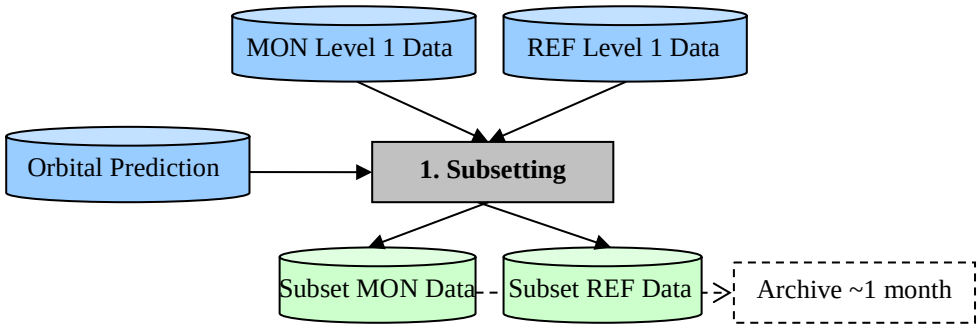

Figure 2: Step 1 of Generic Data Flow, showing inputs and outputs.
MON refers to the monitored instrument. REF refers to the reference instrument.

1.a. *Select Orbit*

1.a.i. Purpose

We first perform a rough cut to reduce the data volume and only include relevant portions of the dataset (channels, area, time and viewing geometry). The purpose is to select portions of data collected by the two instruments that are likely to produce collocations. This is desirable because typically less than 0.1% of measurements are collocated. The processing time is reduced substantially by excluding measurements unlikely to produce collocations.

Data are selected on a per-orbit or per-image basis. To do this, we need to know how often to do inter-calibration – which is based on the observed rate of change and must be defined iteratively with the results of the inter-calibration process (see 5.f).

1.a.ii. General Options

1.a.ii.v0.1. The simplest, but inefficient approach is "trial-and-error", i.e., compare the time and location of all pairs of files within a given time window.

1.a.ii.v0.2. A more sophisticated option is to use the observed orbital parameters (such as the Two Line Elements or TLE) with orbit prediction software such as Simplified General Perturbations Satellite Orbit Model 4 (SGP4). For instrument that has fixed or stable scan pattern such that the measurement time and location are determined by the satellite locations, this is very effective.

1.a.iii. Infrared GEO-LEO inter-satellite/inter-sensor Class

1.a.iii.v0.1. For inter-calibrations between geostationary and sun-synchronous satellites, the orbits provide collocations near the GEO Sub-Satellite Point (SSP) within fixed time windows every day and night. In this case, we adopt the simple approach outlined in general option v0.1.

We define the GEO Field of Regard (FoR) as an area close to the GEO SSP, which is viewed by the GEO sensor with a zenith angle less than a threshold. Wu [2009] defined a threshold angular distance from nadir of less than 60° based on geometric considerations, which is the maximum incidence angle of most LEO sounders. This corresponds to ≈ ±52° in latitude and longitude from the GEO SSP. The GEO and LEO data is then subset to only include observations within this FoR within each inter-calibration period.

Mathematically, the GEO FoR is the collection of locations whose arc angle (angular distance) to nadir is less than a threshold or, equivalently, the cosine of this angle is larger than **min_cos_arc**. We chose the threshold **min_cos_arc = 0.5**, i.e., angular distance less than **60 degrees**.

Computationally, with known Earth coordinates of the Earth center *O*, the North Pole *N*, GEO nadir *G* (0, geo_nad_lon) and the granule center *P* (gra_ctr_lat, gra_ctr_lon), and approximating the Earth as being spherical, the arc angle between a LEO pixel and LEO nadir can be computed with cosine theorem for a right angle on a sphere (see Figure 3):

Equation 1: $\cos(GP) = \cos(gra\_ctr\_lat)\cos(geo\_nad\_lon - gra\_ctr\_lon)$

If the LEO pixel is outside of GEO FoR, no collocation is considered possible. Note the arc angle *GP* on the left panel of Figure 3, which is the same as the angle $\angle GOP$ on the right panel, is smaller than the angle $\angle SPZ$ (right panel, *S* is the GEO position), the zenith angle of GEO from the pixel. This means that the instrument zenith angle is always less than 60 degrees for all collocations.

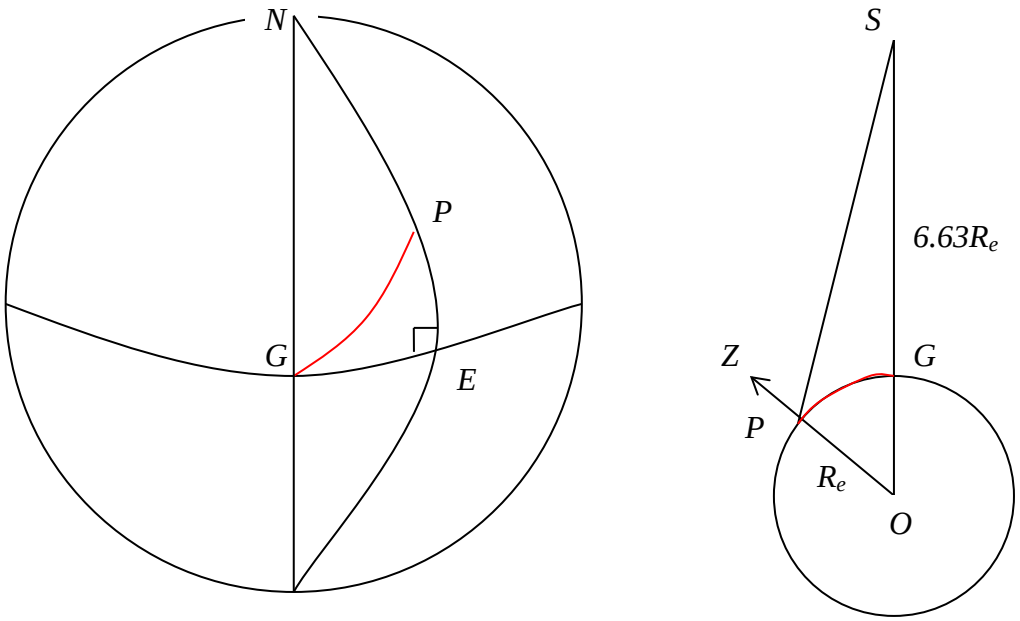

Figure 3: Computing arc angle to satellite nadir and zenith angle of satellite from Earth location

1.a.iv. MTSAT/Himawari-AIRS/IASI Specific

FoR of imagers on MTSAT and Himawari satellites are reduced to include only data within ±30° lat/lon of the SSP. As for the AIRS data, all metadata files of Aqua granules data are downloaded from NASA Goddard Earth Sciences Data and Information Services Center (GES DISC) to specify AIRS granules which cover the GEO FoR. Then the granule data of AIRS L1b which satisfy the condition for match-up are downloaded from the same server. As for the IASI data, TLE (Two-Line Element) data is downloaded from NORAD to predict the orbital time of Metop to be within the FoR. Then the granule data of IASI L1C which satisfy the condition for match-up are downloaded from NOAA Comprehensive Large Array-data Stewardship System (CLASS).

2. **Find Collocations**

A set of observations from a pair of instruments within a common period (e.g. 1 day) is required as input to the algorithm. The first step is to obtain these data from both instruments, select the relevant comparable portions and identify the pixels that are spatially collocated, temporally concurrent, geometrically aligned and spectrally compatible and calculate the mean and variance of these radiances.

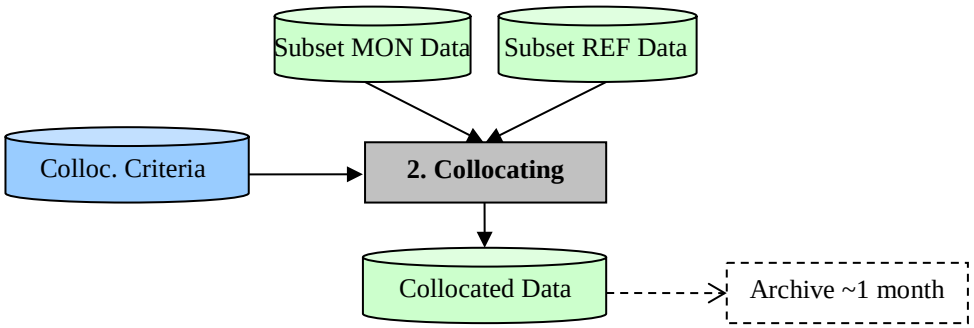

Figure 4: Step 2 of Generic Data Flow, showing inputs and outputs

2.a. *Collocation in Space*

2.a.i. Purpose

The following components of the first step define which pixels can be used in the direct comparison. To do this, we first extract the central location of each instruments' pixels and determine which pixels can considered to be collocated, based on their centers being separated by less than a pre-determined threshold distance. At the same time we identify the pixels that define the *target area* and *environment* around each collocation. These are later averaged in 3.c.

The *target area* is defined to be a little larger than the Field of View (FoV) of the instruments so it covers all the contributing radiation in event of small navigation errors, while being large enough to ensure reliable statistics of the variance are available. The exact ratio of the target area to the FoV will be instrument-specific, but in general will range 1 to 3 times the FoV, with a minimum of 9 'independent' pixels.

2.a.ii. General Options

2.a.ii.v0.1. Each pixel in both instruments' datasets is tested sequentially to identify those separated by less than a pre-determined threshold. Surrounding pixels are used to define the collocation *target area* and *environment*.

2.a.ii.v0.2. A more efficient method of searching for collocations is to calculate 2D-histograms of the locations of both instruments' observations on a common grid in latitude/longitude space. Non-zero elements of both histograms identify the location of collocated pixels and their indices provide the coordinates in observation space (scan line, element, FoV, …).

2.a.ii.v0.3. v0.2 does not capture pixel pairs that straddle bin boundaries of the histograms. This may be refined in future by repeating the histograms on 4 staggered grids, offset by half of the grid spacing, and rationalising the list of collocated pixels returned by the 4 independent searches to remove any duplication (Not implemented yet).

2.a.ii.v0.4. Where instrument's observation pixels follow fixed geographic coordinates, it is possible to use a look-up table to which identify pixels match a given target's location. This is the most efficient and recommended option where available (often for geostationary instruments).

2.a.iii. Infrared GEO-LEO inter-satellite/inter-sensor Class

2.a.iii.v0.1. The spatial collocation criteria are based on the nominal radius of the LEO FoV at nadir. This is taken as a threshold for the maximum distance between the center of the LEO and GEO pixels for them to be considered spatially collocated. However, given the geometry of the already subset data, it is assumed that all LEO pixels within the GEO FoR will be within the threshold distance from a GEO pixel. The GEO pixel closest to the center of each LEO FoV can be identified using a reverse look-up-table (e.g. using a McIDAS function).

2.a.iv. MTSAT/Himawari-AIRS/IASI Specific

AIRS FoV is defined as a circle of 13.5 km diameter at nadir. IASI FoV is defined as a circle of 12 km diameter at nadir. For AIRS/IASI pixels within the GEOT FoR, GEO pixels nearest to the center of each AIRS/IASI pixel are searched.

2.a.iv.1. MTSAT-1R/-2 Specific

MTSAT FoV is defined as square pixels with dimension of 4 x 4 km at the SSP. An array of 3 x 3 MTSAT pixels centered on the pixel closest to center of each AIRS/IASI pixel are defined as *target area*. MTSAT radiances in *target area* are averaged to compare with the AIRS/IASI radiance. The *environment* is defined as 9 x 9 MTSAT pixels centered on its *target area*.

2.a.iv.2. Himawari-8/-9 Specific

AHI FoV is defined as square pixels with dimension of 2 x 2 km at the SSP. An array of 7 x 7 AHI pixels centered on the pixel closest to center of each AIRS/IASI pixel are defined as *target area*. AHI radiances in *target area* are averaged to compare with the AIRS/IASI radiance. The *environment* is defined as 21 x 21 AHI pixels centered on its *target area*.

2.b. *Concurrent in Time*

2.b.i. Purpose

Next we need to identify which of those pixels identified in the previous step as spatially collocated are also collocated in time. Although even collocated measurements at very different times may contribute to the inter-calibration, if treated properly, the capability of processing collocated measurements is limited and the more closely concurrent ones are more valuable for the inter-calibration.

2.b.ii. General Options

Each pixel identified as being spatially collocated is tested sequentially to check whether the observations from both instruments were sampled sufficiently closely in time – i.e. separated in time by no more than a specific threshold. This threshold should be chosen to allow a sufficient number of collocations, while not introducing excessive noise due to temporal variability of the target radiance relative to its spatial variability on a scale of the collocation target area – see Hewison [2009].

2.b.iii. Infrared GEO-LEO inter-satellite/inter-sensor Class

2.b.iii.v0.1. The time at which each collocated pixel of the GEO image was sampled is extracted or calculated and compared to for the collocated LEO pixel. If the difference is greater than a threshold of 300s, the collocation is rejected, otherwise it is retained for further processing.

Equation 2: $\left|LEO\_time - GEO\_time\right| < \max\_\sec$, where *max_sec*=300s

2.b.iii.v0.2. The problem with applying a time collocation criteria in the above form is that it will often lead to only a part of the collocated pixels being analysed. As the GEO image is often climatologically asymmetric about the equator, this can lead to the collocated radiances having different distributions, which can affect the results. A possible solution to this problem is to apply the time collocation to the average sample time of both the GEO and LEO data. This would ensure either all or none of the pixels within each overpass are considered to be collocated in time.

2.b.iv. MTSAT/Himawari-AIRS/IASI Specific

2.b.iv.1. **MTSAT-1R/-2 Specific**

Implemented as 2.b.iii.v0.1

2.b.iv.2. **Himawari-8/-9 Specific**

Implemented as 2.b.iii.v0.1

2.c. *Alignment in Viewing Geometry*

2.c.i. Purpose

The next step is to ensure the selected collocated pixels have been observed under comparable conditions. This means they should be aligned such that they view the surface at similar incidence angles (which may include azimuth and polarisation as well as elevation angles) through similar atmospheric paths.

2.c.ii. General Options

Each pixel identified as being spatially and temporally collocated is tested sequentially to check whether the viewing geometry of the observations from both instruments was sufficiently close. The criterion for zenith angle is defined in terms of atmospheric path length, according to the difference in the secant of the observations' zenith angles and the difference in azimuth angles. If these are less than pre-determined thresholds the collocated pixels can be considered to be aligned in viewing geometry and included in further analysis. Otherwise they are rejected.

2.c.iii. Infrared GEO-LEO inter-satellite/inter-sensor Class

2.c.iii.v0.1. The geometric alignment of infrared channels depends only on the zenith angle and not azimuth or polarisation except for observations during the daytime by short wave infrared channels which contain solar radiation.

Equation 3: $$\left|\frac{\cos(geo\_zen)}{\cos(leo\_zen)} - 1\right| < \max\_zen$$

The azimuth angle [-pi, pi] is defined as the angle rotated clockwise from true north to the satellite line-of-sight projected on the earth surface or, more precisely, the plane tangent on the earth surface at the pixel. It can be computed as illustrated in Figure 3 (left panel). After computing the arc angle GP with Equation 1, one can apply the sine theorem of spherical trigonometry to the arbitrary triangle GPN (the right panel of Figure 3):

Equation 4: $$\sin(GPN) = \sin(geo\_nad\_lon - gra\_ctr\_lon)/\sin(GP)$$

since sin(*NG*) = 1. Thus:

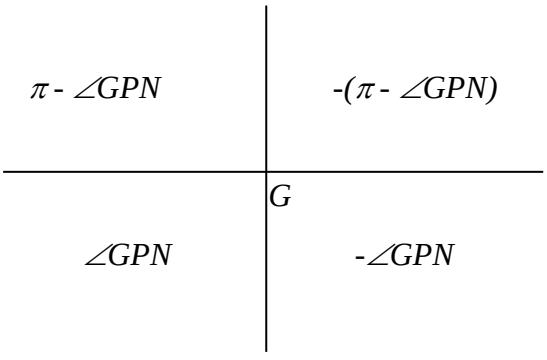

Figure 5: Computation of azimuth angle.

The threshold value for *max_zen* can be quite large for window channels (e.g., 0.05 for 10.8 μm channel) but must be rather small for more absorptive channels (e.g., <0.02 for 13.3 μm channel). Unless there are particular needs to increase the sample size for window channels, a common threshold value of *max_zen*=0.01 is recommended for all channels. This results in collocations being distributed approximately symmetrically about the equator mapping out a characteristic *slanted hourglass* pattern.

Another aspect of viewing geometry alignment is azimuth angle. Similar zenith angle assures similar path length; additional requirement of similar azimuth angle assures similar line-of-sight. Line-of-sight alignment is relevant for IR spectrum in certain cases. For infrared window channels, land surface emission during daytime may be anisotropic [Minnis *et al.* 2004]. For shortwave IR band (e.g., 4 μm), azimuth angle alignment is required during daytime when solar radiation is considerable. It is, therefore recommended that inter-calibration over land and in this band is limited to night-time only cases – at the expense of limiting the dynamic range of the results.

2.c.iv. MTSAT/Himawari-AIRS/IASI Specific

The method is similar to 2.c.iii.v0.1., but the equation used for checking the zenith angle is slightly different from Equation 3. The threshold value for max_*zen* differs according to channels and weather conditions. In this method, if the brightness temperature of thermal infrared channel (e.g. IR1 of MTSAT: 10.8 μm) is higher than 275 K, the scene condition is categorized as clear. Otherwise, it is categorized as cloudy.

Equation 5: $$\left|\frac{\cos(leo\_zen)}{\cos(geo\_zen)} - 1\right| < \max\_zen$$

2.c.iv.1. MTSAT-1R/-2 Specific

The following values are used for max_*zen*.
IR1, IR2, IR4: 0.01 (clear)
IR1, IR2, IR4: 0.03 (cloudy)
IR3: 0.01 (all)

2.c.iv.2. Himawari-8/-9 Specific

The following values are used for max_*zen*.
B07, B11, B12, B13, B14, B15, B16: 0.01 (clear)
B07, B11, B12, B13, B14, B15, B16: 0.03 (cloudy)
B08, B09, B10: 0.01 (all)

2.d. *Pre-Select Channels*

2.d.i. Purpose

Only broadly comparable channels from both instruments are selected to reduce data volume.

2.d.ii. General Options

2.d.ii.v0.1. This selection is based on pre-determined criteria for each instrument pair.

2.d.iii. Infrared GEO-LEO inter-satellite/inter-sensor Class

2.d.iii.v0.1. Only the channels of the GEO and LEO sensors are selected in the thermal infrared range of 3-15μm.

2.d.iv. MTSAT/Himawari-AIRS/IASI Specific

Select only the short-wave infrared, water vapour and thermal infrared channels of GEO sensors. Select all channels for AIRS/IASI.

2.d.iv.1. **MTSAT-1R/-2 Specific**

Select MTSAT's infrared channels: IR1, IR2, IR3 and IR4.

2.d.iv.2. **Himawari-8/-9 Specific**

Select AHI's infrared bands: B07, B08, B09, B10, B11, B12, B13, B14, B15 and B16.

2.e. *Plot Collocation Map*

2.e.i. Purpose

When interpreting the inter-calibration results it is often helpful to visualise the distribution of the source data used in the comparison.

2.e.ii. General Options

This can be achieved by producing a map showing the distribution of collocation targets.

2.e.iii. Infrared GEO-LEO inter-satellite/inter-sensor Class

2.e.iii.v0.1. The map is produced showing all the GEO-LEO pixels meeting the collocation criteria every day. These points are overlaid on a background image from an infrared window channel of the GEO instrument. This allows the distribution of cloud to be visualised and considered in the interpretation of the results.

2.e.iv. MTSAT/Himawari-AIRS/IASI Specific

2.e.iv.1. MTSAT-1R/-2 Specific

Not yet implemented.

2.e.iv.2. Himawari-8/-9 Specific

Not yet implemented.

3. **Transform Data**

In this step, collocated data are transformed to allow their direct comparison. This includes modifying the spectral, temporal and spatial characteristics of the observations, which requires knowledge of the instruments' characteristics. The outputs of this step are the best estimates of the channel radiances, together with estimates of their uncertainty.

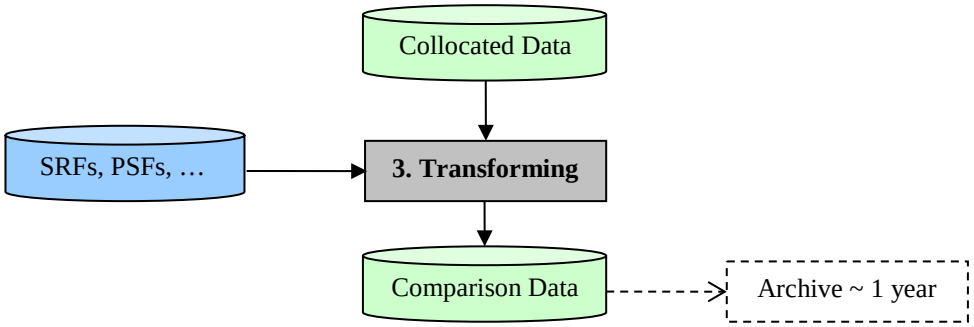

Figure 6: Step 3 of Generic Data Flow, showing inputs and outputs.

3.a. *Convert Radiances*

3.a.i. Purpose

Convert observations from both instruments to a common definition of radiance to allow direct comparison.

3.a.ii. General Options

3.a.ii.v0.1. The instruments' observations are converted from Level 1.5/1b/1c data to radiances, using pre-defined, published algorithms specific for each instrument.

3.a.iii. Infrared GEO-LEO inter-satellite/inter-sensor Class

3.a.iii.v0.1. Perform comparison in radiance units: $mW/m^2/sr/cm^{-1}$.

3.a.iv. MTSAT/Himawari-AIRS/IASI Specific

3.a.iv.1. MTSAT-1R/-2 Specific

Implemented as 3.a.iii.v0.1. The MTSAT HRIT data contain a look-up table to convert digital number to brightness temperature. The brightness temperatures are converted to radiances by the sensor Planck function in Tahara [2008a].

3.a.iv.2. Himawari-8/-9 Specific

Implemented as 3.a.iii.v0.1. AHI radiance data in wavelength units ($W/m^2/sr/\mu m$) can be converted from digital number in Himawari Standard Data (HSD). The radiances are converted to brightness temperatures using conversion coefficients in HSD. Then, the brightness temperatures are converted to the radiances in wavenumber units ($mW/m^2/sr/cm^{-1}$) using the sensor Planck function in the Appendix. The conversion coefficients are also available in the GSICS Correction netCDF file and online[1].

[1] http://www.data.jma.go.jp/mscweb/data/monitoring/gsics/ir/techinfo_geoleoir.html (last access on 10 August 2017)

3.b. *Spectral Matching*

3.b.i. Purpose

Firstly, we must identify which channel sets provide sufficient common information to allow meaningful inter-calibration. These are then transformed into comparable pseudo channels, accounting for the deficiencies in channel matches.

3.b.ii. General Options

3.b.ii.v0.1. The Spectral Response Functions (SRFs) must be defined for all channels. The observations of channels identified as comparable are then co-averaged using pre-determined weightings to give *pseudo channel* radiances. A Radiative Transfer Model can be used to account for any differences in the pseudo channels' characteristics. The uncertainty due to spectral mismatches is then estimated for each channel.

3.b.iii. Infrared GEO-LEO inter-satellite/inter-sensor Class

For hyper-spectral instruments, all SRFs are first transformed to a common spectral grid. The LEO hyperspectral channels are then convolved with the GEO channels' SRFs to create synthetic radiances in pseudo-channels, accounting for the spectral sampling and stability in an error budget.

Equation 6: $$R_{GEO} = \frac{\int_{\nu} R_{\nu} \Phi_{\nu} d\nu}{\int_{\nu} \Phi_{\nu} d\nu}$$

where R_{GEO} is the simulated GEO radiance, R_{ν} is LEO radiance at wave number ν, and Φ_{ν} is GEO spectral response at wave number ν.

In general LEO hyperspectral sounders do not provide complete spectral coverage of the GEO channels either by design (e.g. gaps between detector bands), or by subsequent hardware failure (e.g. broken or noisy channels). The radiances in these *gap channels* shall be accounted by one of the following techniques:

3.b.iii.v0.1. The simplest option is simply to ignore the contribution from the *gap channels.* This will obviously introduce a bias in the resulting radiances, depending on the specific channels under consideration.

3.b.iii.v0.2. A second option is to linearly interpolate for the missing radiance from the adjacent valid channels. This could be a viable option for narrow gaps (e.g., single dead or unstable channel) but would create large bias and uncertainty if the gap is wide and over complex spectral features.

3.b.iii.v0.3. Tobin et al. [2006] fills the gap with pre-computed radiance using a radiative transfer model (RTM) and some typical atmospheric profiles. This is a significant improvement over the previous options, but the error can be large at times since spectral radiance is dependent on atmospheric conditions such as clouds, which is not known *a priori*.

3.b.iii.v0.4. The method of Tahara [2008b] exploits the fact that spectral radiances are normally highly correlated. It fills the gap with pre-computed radiance adjusted by ratio of measured and pre-computed radiances at nearby channels.

3.b.iii.v0.5. Gunshor et al. [2009] matches the pre-computed radiance at the beginning and end of the gap. The ratio between the AIRS radiance and simulated radiance is computed at the last channel before a gap and the first channel after the gap, and is linearly interpolated to the channels within the gap. The missing AIRS radiances are then estimated as the simulated radiances multiplied with the ratio linearly interpolated to the missing channel.

3.b.iii.v0.6. **This is the recommended option.** Tahara and Kato [2009] define virtual channels named *gap channels* to fill the spectral gaps and introduce the spectral compensation method by constrained optimization. The gap channels to fill the AIRS spectral gaps (AIRS gap channels) are defined by 0.5 cm^{-1} intervals, and are characterized by a unique SRF, whose shape is a Gaussian curve with a sigma of 0.5 cm^{-1}. The gap channels to extend the IASI spectral region (IASI gap channels) are defined by the same intervals (0.25 cm^{-1}) and SRFs as the IASI level 1c channels. The radiances of the missing channels are calculated by regression analysis using radiative transfer simulated radiances with respect to the eight atmospheric model profiles as explanatory variables.

Equation 7: $$\log I_i^{calc} = c_0 + \sum_{k=1}^{K} c_k \log I_{i,k}^{sim} \left(i = \textit{hyper and gap channels}\right),$$

where I_i^{calc} is the calculated radiance of the hyper channel *i*, $I_{i,k}^{sim}$ is the simulated radiance of the hyper channel *i* with respect to the atmospheric model profile *k*, $c_k \left(k = 1, \ldots, K\right)$ are regression coefficients, and *K* is the number of the atmospheric model profiles. Equation 7 introduces logarithm radiances as response and explanatory variables in order to increase fitting accuracy and avoid calculation of negative radiance. The regression coefficients c_k are independent of the hyper channels, and are generated for each scan position of the hyper sounder. c_k are obtained by the least-square method applying a set of validly observed radiances I_i^{obs} in place of I_i^{calc} to Equation 7,

Equation 8: $$\{c_k\} = \arg\min \sum_{i=exist(I_i^{obs})} \left\{ \log I_i^{obs} - \left(c_0 + \sum_k c_k \log I_{i,k}^{sim} \right) \right\}^2 .$$

Once the regression coefficients c_k are computed, the radiances of the missing channels can be calculated by Equation 7. It might be possible to apply the observed radiances of all hyper channels to Equation 8 to compute c_k and then calculate the radiances of all missing channels at once. However, this yields a large fitting error in practice. In inter-calibration application, the coefficients c_k are computed for each broadband channel spectral region. Equation 7 and Equation 8 use the simulated radiances $I_{i,k}^{sim}$. For the radiance simulation, this study uses the following eight atmospheric model profiles:

1. U.S. standard without cloud,
2. U.S. standard with opaque cloud with tops at 500 hPa altitude,
3. U.S. standard with opaque cloud with tops at 200 hPa altitude,

4. Tropical without cloud,
5. Tropical with opaque cloud with tops at 500 hPa altitude,
6. Tropical with opaque cloud with tops at 200 hPa altitude,
7. Mid-latitude summer without cloud,
8. Mid-latitude winter without cloud.

These profiles include not only clear sky conditions but also cloudy conditions because Equation 7 should be applicable under any weather conditions. As for radiative transfer code, the line-by-line code LBLRTM (Clough et al., 1995) version 11.1 is used with the HITRAN2004 spectroscopy line parameter database (Rothman et al., 2003) including the AER updates version 2.0 (AER Web page). The emissivities of the surface and clouds are assumed to be one. The benefit of this spectral compensation method is that it does not require radiative transfer computation to be run in inter-calibration operation. This not only speeds up the computation but also prevents super channel radiance computation from introducing biases contained in radiative transfer code and atmospheric state fields.

3.b.iv. MTSAT/Himawari-AIRS/IASI Specific

The gap channels to fill the AIRS spectral gaps (AIRS gap channels) are defined by 0.5 cm^{-1} interval, and are characterized by a unique SRF, whose shape is a Gaussian curve with a sigma of 0.5 cm^{-1}. For IASI, the gap channels to extend the IASI spectral region (IASI gap channels) are defined by the same intervals (0.25 cm^{-1}) and SRFs as the IASI level 1c channels.

3.b.iv.1. **MTSAT-1R/-2 Specific**

Implemented as 3.b.iii.v0.6.

3.b.iv.2. **Himawari-8/-9 Specific**

Implemented as 3.b.iii.v0.6.

3.c. *Spatial Matching*

3.c.i. Purpose

The observations from each instrument are transformed to comparable spatial scales. This involves averaging all the pixels identified in 2 as being within the *target* and *environment* areas. The uncertainty due to spatial variability is estimated.

3.c.ii. General Options

3.c.ii.v0.1. The Point Spread Functions (PSFs) of each instrument are identified. The *target area* and *environment* around it were specified in 2. Now the pixels within these areas are identified and their radiances are averaged and their variance calculated to estimate the uncertainty on the average due to spatial variability, accounting for any over-sampling.

3.c.iii. Infrared GEO-LEO inter-satellite/inter-sensor Class

3.c.iii.v0.1. The *target area* is defined as the nominal LEO FoV at nadir. The GEO pixels within target area are averaged using a uniform weighting and their variance calculated. The *environment* is defined by the GEO pixels within 3x radius of the *target area* from the center of each LEO FoV. Observation information in the *target area* and the *environment* are used for uniformity tests in 4.

3.c.iii.v0.2. The Point Spread Function (PSF) of the LEO instrument is used to provide a weighting in calculating the average of the GEO pixels (Not implemented yet).

3.c.iv. MTSAT/Himawari-AIRS/IASI Specific

As above, the AIRS and IASI FoV are defined as a circle of 13.5 km and 12 km diameter at nadir, respectively.

3.c.iv.1. MTSAT-1R/-2 Specific

As described in 2.a.iv.1, the MTSAT FoVs for infrared channels are defined nominally as square pixels with lengths of 4km at SSP, which are assumed to be constant across the swath of each instrument. The *target area* is defined by arrays of 3 x 3 MTSAT pixels closest to center of each AIRS/IASI FoV. The *environment* is defined by an array 9 x 9 MTSAT pixels, centered on the AIRS/IASI FoV.

3.c.iv.2. Himawari-8/-9 Specific

As described in 2.a.iv.2, the AHI FoVs for infrared bands are defined nominally as square pixels with lengths of 2km at SSP, which are assumed to be constant across the swath of each instrument. The *target area* is defined by arrays of 7 x 7 AHI pixels closest to center of each AIRS/IASI FoV. The *environment* is defined by an array 21 x 21 AHI pixels, centered on the AIRS/IASI FoV.

3.d. *Viewing Geometry Matching*

3.d.i. Purpose

Despite the collocation criteria described in 2.c, each instrument can measure radiance from the collocation targets in slightly different viewing geometry. It may be possible to account for small differences by considering simplified a radiative transfer model.

3.d.ii. General Options

3.d.ii.v0.1. Differences in viewing geometry within the collocation criteria described in 2.c are assumed to be negligible and ignored in further analysis.

3.d.ii.v0.2. It may be possible to account for small differences by considering simplified a radiative transfer model.

3.d.iii. Infrared GEO-LEO inter-satellite/inter-sensor Class

3.d.iii.v0.1. Differences in viewing geometry within the collocation criteria described in 2.c are assumed to be negligible and ignored in further analysis.

3.d.iii.v0.2. It may be possible to account for small differences by considering simplified a radiative transfer model (Not yet implemented).

3.d.iv. MTSAT/Himawari-AIRS/IASI Specific

3.d.iv.1. **MTSAT-1R/-2 Specific**

Implemented as 3.d.iii.v0.1.

3.d.iv.2. **Himawari-8/-9 Specific**

Implemented as 3.d.iii.v0.1.

3.e. *Temporal Matching*

3.e.i. Purpose

Different instruments measure radiance from the collocation targets at different times. The impact of this difference can usually be reduced by careful selection, but not completely eliminated. The timing difference between instruments' observations is established and the uncertainty of the comparison is estimated based on (expected or observed) variability over this timescale.

3.e.ii. General Options

3.e.ii.v0.1. Each instrument's sample timings are identified.

3.e.iii. Infrared GEO-LEO inter-satellite/inter-sensor Class

3.e.iii.v0.1. Only the GEO image closest to the LEO equator crossing time is selected. The time difference between the collocated GEO and LEO observations is neglected and the collocation targets are assumed to be sampled simultaneous, contributing no additional uncertainty to the comparison.

3.e.iii.v0.2. Only the GEO image closest to the LEO Equator crossing time is selected. The time difference, Δt, between the collocated GEO and LEO observations is calculated for each collocated pixel. This is compared with the spatial distance between the centroids of the target areas sampled by GEO and LEO, Δx, defined in 3.c using the pre-determined relationship between spatial and temporal scene variability for this channel [Hewison, 2009] and the uncertainty due to temporal variability, σ_t, is estimated from that due to spatial variability, σ_x, calculated in 3.c.

Equation 9: $\sigma_t = \left(\frac{RMSD_t(\Delta t)}{RMSD_x(\Delta x)} \right) \sigma_x$,

where $RMSD_t(\Delta t)$ and $RMSD_x(\Delta x)$ are the r.m.s. differences between the radiances in each channel calculated for sampling period, Δt, and interval, Δx, respectively (Not yet implemented).

3.e.iii.v0.3. Sequential GEO images are interpolated to the LEO observation time and weighted according to the time difference between each. The uncertainty of the weighted mean could also be estimated (Not yet implemented).

3.e.iv. MTSAT/Himawari-AIRS/IASI Specific

3.e.iv.1. **MTSAT-1R/-2 Specific**

Implemented as 3.e.iii.v0.1.

3.e.iv.2. **Himawari-8/-9 Specific**

Implemented as 3.e.iii.v0.1.

4. **Filtering**

The collocated and transformed data will be archived for analysis. Before that, the GSICS inter-calibration algorithm reserves the opportunity to remove certain data that should not be analyzed (quality control), and to add auxiliary data that will add further analysis. For example, it may be useful to incorporate land/sea/ice masks and/or cloud flags to better classify the results.

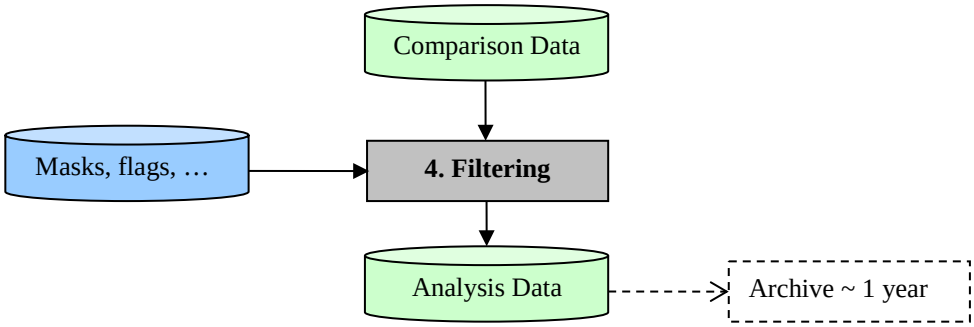

Figure 7: Step 4 of Generic Data Flow, showing inputs and outputs.

4.a. *Uniformity Test*

4.a.i. Purpose

Knowledge of scene uniformity is critical in reducing and evaluating inter-calibration uncertainty. To reduce uncertainty in the comparison due to spatial/temporal mismatches, the collocation dataset may be filtered so only observations in homogenous scenes are compared.

4.a.ii. General Options

4.a.ii.v0.1. The simplest option is to allow all inter-calibration targets, regardless of their uniformity.

4.a.ii.v0.2. Another option is to set threshold to allow only relatively uniform scenes for analysis. In this case, the spatial/temporal variability of the scene within the target area is compared with pre-defined thresholds to exclude scenes with greater variance from analysis. This may be performed on a per-channel basis.

4.a.ii.v0.3. Another option is to use scene uniformity as weight in further analysis. Comparatively, the threshold option has the theoretical disadvantage of subjectivity but practical advantage of substantially reducing the amount of data to be archived. Recent analysis [Tobin, personal communication, 2009] also indicates that the threshold option is always suboptimal compared to the weight option.

4.a.iii. Infrared GEO-LEO inter-satellite/inter-sensor Class

4.a.iii.v0.1. The variance of the radiances of all the GEO pixels within each LEO FoV is calculated in 3.c.

4.a.iii.v0.2. The interpolation between sequential GEO images may be included in future (Not yet implemented).

4.a.iv. MTSAT/Himawari-AIRS/IASI Specific

The *target area* and *environment* defined in 3.c are used. To mitigate differences between the observation conditions of the two satellites due to time difference, optical path difference, image navigation error and so on, only measurements over uniform scenes are selected and compared. In this *environment* uniformity check, the uniformity of GEO radiance data in the *environment* is tested using

Equation 10: $STDV(ENV) < \max\_STDV$ **,**

where *STDV(ENV)* means standard deviation of GEO radiances in the *environment*.

LEO radiance is compared to the averaged GEO radiance in the *target area*. The GEO radiance data in the *target area* should therefore represent the data in the *environment* evaluated by the *environment* uniformity check. The normality of the GEO radiance data in the *target area* is checked using

Equation 11: $\left|MEAN(TARGET) - MEAN(ENV)\right| \times \frac{FOVLEN(TARGET)}{STDV(ENV)} < Gaussian.,$

where *MEAN(TARGET)* and *MEAN(ENV)* are mean of GEO radiances in the *target area* and *environment*, respectively. *FOVLEN(TARGET)* is a length (i.e. number of pixels) of *target area*.

The thresholds for max_*STDV* and *Gaussian* differ according to channels and weather conditions. In this version, if the brightness temperature of thermal infrared channel (i.e. IR1 for MTSAT and B13 for AHI) is higher than 275 K, the scene condition is categorized as clear. Otherwise, it is categorized as cloudy. This is same with 0.

4.a.iv.1. **MTSAT-1R/-2 Specific**

The following are max_*STDV* [mW/(m^2.sr.cm^{-1})] and *Gaussian* values. *FOVLEN(TARGET)* is 3.

	IR1 (10.8 μm)		IR2 (12.0 μm)		IR3 (6.8 μm)		IR4 (3.8 μm)	
max_STDV	clear	cloudy	clear	cloudy	clear	cloudy	clear	cloudy
	1.65	3.31	1.82	3.64	0.311		0.0151	0.0302
Gaussian	2		2		1		2	

4.a.iv.2. **Himawari-8 Specific**

The following are max_*STDV* [mW/(m^2.sr.cm^{-1})] and *Gaussian* values. *FOVLEN(TARGET)* is 7.

	B07 (3.9 μm)		B08 (6.2 μm)		B09 (6.9 μm)		B10 (7.3 μm)		B11 (8.6 μm)	
max_STDV	clear	cloudy	clear	cloudy	clear	cloudy	clear	cloudy	clear	cloudy
	0.0238	0.0476	0.371		0.561		0.661		1.18	2.36
Gaussian	2		1		1		1		2	

	B12 (9.6 μm)		B13 (10.4 μm)		B14 (11.2 μm)		B15 (12.4 μm)		B16 (13.3 μm)	
max_STDV	clear	cloudy	clear	cloudy	clear	cloudy	clear	cloudy	clear	cloudy
	1.46	2.92	1.62	3.24	1.77	3.54	1.91	3.82	2.03	4.06
Gaussian	2		2		2		2		2	

4.a.iv.3. **Himawari-9 Specific**

The following are max_*STDV* [mW/(m^2.sr.cm^{-1})] and *Gaussian* values. *FOVLEN(TARGET)* is 7.

	B07 (3.9 μm)		B08 (6.2 μm)		B09 (6.9 μm)		B10 (7.3 μm)		B11 (8.6 μm)	
max_STDV	clear	cloudy	clear	cloudy	clear	cloudy	clear	cloudy	clear	cloudy
	0.0217	0.0434	0.372		0.565		0.661		1.18	2.36
Gaussian	2		1		1		1		2	

	B12 (9.6 μm)		B13 (10.4 μm)		B14 (11.2 μm)		B15 (12.4 μm)		B16 (13.3 μm)	
max_STDV	clear	cloudy	clear	cloudy	clear	cloudy	clear	cloudy	clear	cloudy
	1.46	2.92	1.62	3.24	1.76	3.52	1.91	3.82	2.03	4.06
Gaussian	2		2		2		2		2	

4.b. *Outlier Rejection*

4.b.i. Purpose

To prevent anomalous observations having undue influence on the results, 'outliers' may be identified and rejected on a statistical basis. Small number of anomalous pixels in the environment, even concentrated, may not fail the uniformity test. However, if they appear only in one sensor's field of view but not the other, it can cause unwanted bias in a single comparison.

4.b.ii. General Options

4.b.ii.v0.1. The simplest implementation is to include the outliers in the further analysis. Since the anomaly has equal chance to appear in either sensor's field of view, comparison of large number of samples remains unbiased but has increased noise. This is the recommended approach.

4.b.ii.v0.2. The radiances in the target area are compared with those in the surrounding *environment*, and those targets which are significantly different from the environment (3σ) may be rejected. For a normally distributed population of size *N*, mean *M*, and standard deviation *S*, the difference between a single sample and *M* has the probability of ~68% to be less than *S*, ~95% to be less than 2*S*, and so forth. Similarly, the difference between the mean of n^2 samples and *M* has the probability of ~68% to be less than $S/n[(N-n)/(N-1)]$, ~95% to be less than $2S/n[(N-n)/(N-1)]$, and so forth. This property is used to test whether the collocation area is an outlier for the otherwise uniform environment:

Equation 12: $$\left|\frac{1}{n^2}\sum_{i=1}^{n^2} R_i - M\right| \le \frac{S}{n}\frac{N-n}{N-1}Gaussian(=3)$$

where R is radiance from individual pixel, n2 is the number of samples, and Gaussian is a threshold. The probability that the rejected sample is an outlier is 68% if *Gaussian*=1, 95% if *Gaussian*=2, and more than 99% if *Gaussian*=3.

4.b.iii. Infrared GEO-LEO inter-satellite/inter-sensor Class

4.b.iii.v0.1. All inter-calibration targets are included in further analysis, regardless of whether they are outliers with respect to their environment.

4.b.iii.v0.2. The mean GEO radiances within each LEO FoV are compared to the mean of their *environment*. Targets where this difference is >3 times the standard deviation of the environment's radiances are rejected.

4.b.iv. MTSAT/Himawari-AIRS/IASI Specific

4.b.iv.1. MTSAT-1R/-2 Specific

Outliers are rejected only for the reference instruments before the comparison. AIRS channels in case that either "ExcludedChans" flag, "CalChanSummary" flag, "CalChanSummary" flag or "CalFlag" indicates any problem are excluded. A radiance data of an AIRS channel in case that either "state" indicates in science mode or the radiance is less 0 [mW/(m^2.sr.cm^{-1})] or larger than 200 [mW/(m^2.sr.cm^{-1})] is excluded. In the case of IASI, a

radiance data of an IASI channel in case that the radiance is less -10 [mW/(m^2.sr.cm^{-1})] or larger than 200 [mW/(m^2.sr.cm^{-1})] is excluded.

4.b.iv.2. **Himawari-8/-9 Specific**

Implemented as 4.b.iv.1.

4.c. *Auxiliary Datasets*

4.c.i. Purpose

It may be useful to incorporate land/sea/ice masks and/or cloud flags to allow analysis of statistics in terms of other geophysical variables – e.g. land/sea/ice, cloud cover, etc.

It may also be possible to estimate the spatial variability within the LEO FoV from collocated AVHRR observations from the same LEO satellite.

4.c.ii. General Options

4.c.ii.v0.1. Not yet implemented.

4.c.iii. Infrared GEO-LEO inter-satellite/inter-sensor Class

4.c.iii.v0.1. Not yet implemented.

4.c.iv. MTSAT/Himawari-AIRS/IASI Specific

4.c.iv.1. MTSAT-1R/-2 Specific

Not yet implemented.

4.c.iv.2. Himawari-8/-9 Specific

Not yet implemented.

5. **Monitoring**

This step includes the actual comparison of the collocated radiances produced in Steps 1-4, the production of statistics summarising the results to be used in the Correcting step, and reporting any differences in ways meaningful to a range of users.

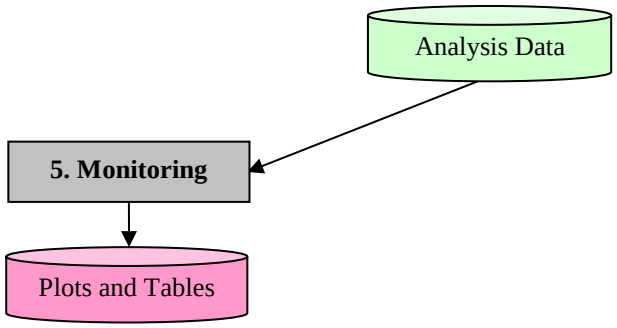

Figure 8: Step 5 of Generic Data Flow, showing inputs and outputs.

5.a. *Define Standard Radiances (Offline)*

5.a.i. Purpose

This component provides standard reference scene radiances at which instruments' inter-calibration bias can be directly compared and conveniently expressed in units understandable by the users. Because biases can be scene-dependent, it is necessary to define channel-specific *standard radiances*. More than one standard radiance may be needed for different applications – e.g. clear/cloudy, day/night. This component is carried out offline.

5.a.ii. General Options

5.a.ii.v0.1. A representative Region of Interest (RoI) is selected and histograms of the observed radiances within RoI are calculated for each channel. Histogram peaks are identified corresponding to clear/cloudy scenes to define standard radiances. These are determined *a priori* from representative sets of observations.

5.a.ii.v0.2. The standard radiances should be calculated for each channel *a priori* using a Radiative Transfer Model (RTM) based on a standard atmospheric profile and surface conditions. The reference radiance should be calculated at nadir, at night for IR channels or at a given solar angle (for vis/nir channels), in a 1976 US Standard Atmosphere, in clear skies, over the sea with a SST=+15C and wind speed (7m/s), using some standard RTM, accounting for the SRF of each channel. This has the advantages of being independent of any instrument biases and provides standard radiances against which we can compare the instruments' relative biases derived from a number of different inter-calibration techniques.

5.a.iii. Infrared GEO-LEO inter-satellite/inter-sensor Class

5.a.iii.v0.1. Option 5.a.ii.v0.1 is implemented directly.

5.a.iii.v0.2. Option 5.a.ii.v0.1 is implemented directly, the FoR is limited to within 30° latitude/longitude of the GEO sub-satellite point and times limited to night-time LEO overpasses.

5.a.iv. MTSAT-AIRS/IASI Specific

5.a.iv.1. MTSAT-1R/-2 Specific

The calculation of standard radiances in 5.a.ii.v0.2 is implemented, using RTTOV-9, giving the following results for the IR channels on MTSAT-1R/JAMI and MTSAT-2/Imager:

	Channel (μm)	IR1(10.8)	IR2(12.0)	IR3(6.8)	IR4(3.8)
MTSAT-1R	T_{bstd} (K)	286.67	285.91	238.37	286.51
MTSAT-2		286.70	285.94	239.17	286.53

5.a.iv.2. Himawari-8/-9 Specific

The calculation of standard radiances in 5.a.ii.v0.2 is implemented, using RTTOV-11, giving the following results for the IR bands on AHIs on Himawari-8/-9 (AHI-8/-9):

	Band (μm)	Band7 (3.9)	Band8 (6.2)	Band9 (6.9)	Band10 (7.3)	Band11 (8.6)	Band12 (9.6)	Band13 (10.4)	Band14 (11.2)	Band15 (12.4)	Band16 (13.3)
AHI-8	T_{bstd} (K)	285.95	234.65	243.85	254.59	283.82	259.45	286.18	286.10	283.78	269.73
AHI-9		286.02	234.75	244.20	254.77	283.88	259.33	286.22	286.16	283.92	268.53

5.b. *Regression of Most Recent Results*

5.b.i. Purpose

Regression is used as the basis of the systematic comparison of collocated radiances from two instruments. (This comparison may also be done in counts or brightness temperature.) Regression coefficients shall be made available to users to apply the GSICS Correction to the monitored instrument, re-calibrating its radiances to be consistent with those of the reference instrument. Scatterplots of the regression data should also be produced to allow visualisation of the distribution of radiances.

Regressions also allow us to investigate how biases depend on various geophysical variables and provides statistics of any significant dependences, which can used to refine corrections and allows investigation of the possible causes. Such investigations should be carried out offline and may result in future refinements to the ATBD.

5.b.ii. General Options

5.b.ii.v0.1. The simplest method of comparing two datasets is to calculate the average the differences between collocated radiances. This provides a single scalar quantity for each channel (with an uncertainty estimated statistically from the variances of the datasets). However, this does not correspond to the mechanisms most likely to introduce bias in the instruments. A weighted average may be used to account for greater uncertainty of collocation with inhomogeneous scene radiances.

5.b.ii.v0.2. Similarly, the average ratio of the collocated radiances from a pair of instruments can be calculated. This also provides a single scalar quantity for each channel (with an uncertainty estimated statistically from the variances of the datasets). This corresponds to an inaccurately calibrated gain of one of the instruments, which is a common problem. A weighted average may be used to account for greater uncertainty of collocation with inhomogeneous scene radiances.

5.b.ii.v0.3. The recommended approach is to perform a weighted linear regression of collocated radiances. The inverse of the sum of the spatial and temporal variance of the target radiance and the radiometric noise provide an estimated uncertainty on each dependent point, which is used as a weighting. (Including the radiometric noise ensures that very homogeneous targets scenes where all the pixels give the same radiance do not have undue influence on the weighted regression.)

This method produces estimates of regression coefficients describing the slope and offset of the relationship between the two instruments' radiances – together with their uncertainties, expressed as a covariance. The problem of correlation between the uncertainties on each coefficient may be reduced by performing the regression on a transformed dataset – for example, by subtracting the mean or reference radiance from each set.

The observations of the reference instrument, *x*, and monitored instrument, *y*, are fitted to a straight line model of the form:

Equation 13: $\hat{y}(x) = a + bx$

We assume an uncertainty σ_i associated with each measurement, y_i, is known and that the dependent variable, x_i is also known.

To fit the observed data to the above model, we minimise the chi-square merit function:

Equation 14: $$\chi^2(a,b) = \sum_{i=1}^{N}\left(\frac{y_i - a - bx_i}{\sigma_i}\right)^2$$

This can be implemented following the method described in Section 15.2 of Numerical Recipes [Press *et al.*, 1996], which is implemented in the *POLY_FIT* function of IDL, yielding the following estimates of the regression coefficients:

Equation 15: $$a = \frac{\sum_{i=1}^{N}\frac{x_i^2}{\sigma_i^2}\sum_{i=1}^{N}\frac{y_i}{\sigma_i^2} - \sum_{i=1}^{N}\frac{x_i}{\sigma_i^2}\sum_{i=1}^{N}\frac{x_i y_i}{\sigma_i^2}}{\sum_{i=1}^{N}\frac{1}{\sigma_i^2}\sum_{i=1}^{N}\frac{x_i^2}{\sigma_i^2} - \left(\sum_{i=1}^{N}\frac{x_i}{\sigma_i^2}\right)^2},$$

Equation 16: $$b = \frac{\sum_{i=1}^{N}\frac{1}{\sigma_i^2}\sum_{i=1}^{N}\frac{x_i y_i}{\sigma_i^2} - \sum_{i=1}^{N}\frac{x_i}{\sigma_i^2}\sum_{i=1}^{N}\frac{y_i}{\sigma_i^2}}{\sum_{i=1}^{N}\frac{1}{\sigma_i^2}\sum_{i=1}^{N}\frac{x_i^2}{\sigma_i^2} - \left(\sum_{i=1}^{N}\frac{x_i}{\sigma_i^2}\right)^2},$$

their uncertainties:

Equation 17: $$\sigma_a^2 = \frac{\sum_{i=1}^{N}\frac{x_i^2}{\sigma_i^2}}{\sum_{i=1}^{N}\frac{1}{\sigma_i^2}\sum_{i=1}^{N}\frac{x_i^2}{\sigma_i^2} - \left(\sum_{i=1}^{N}\frac{x_i}{\sigma_i^2}\right)^2},$$

Equation 18: $$\sigma_b^2 = \frac{\sum_{i=1}^{N}\frac{1}{\sigma_i^2}}{\sum_{i=1}^{N}\frac{1}{\sigma_i^2}\sum_{i=1}^{N}\frac{x_i^2}{\sigma_i^2} - \left(\sum_{i=1}^{N}\frac{x_i}{\sigma_i^2}\right)^2},$$

and their covariance:

Equation 19: $$\mathrm{cov}(a,b) = \frac{-\sum_{i=1}^{N}\frac{x_i}{\sigma_i^2}}{\sum_{i=1}^{N}\frac{1}{\sigma_i^2}\sum_{i=1}^{N}\frac{x_i^2}{\sigma_i^2} - \left(\sum_{i=1}^{N}\frac{x_i}{\sigma_i^2}\right)^2}.$$

5.b.iii. Infrared GEO-LEO inter-satellite/inter-sensor Class

5.b.iii.v0.1. Inter-calibrations are repeated daily using only night-time LEO overpasses. Collocations are weighted by the inverse the sum of the spatial and temporal variance of target radiances and their radiometric noise level in the regression. (The inclusion of the radiometric noise ensures the weights never become infinite due to collocation targets with zero variance.) Scatterplots of the regression data should also be produced to allow visualisation of the distribution of radiances, following the example shown in Figure 9.

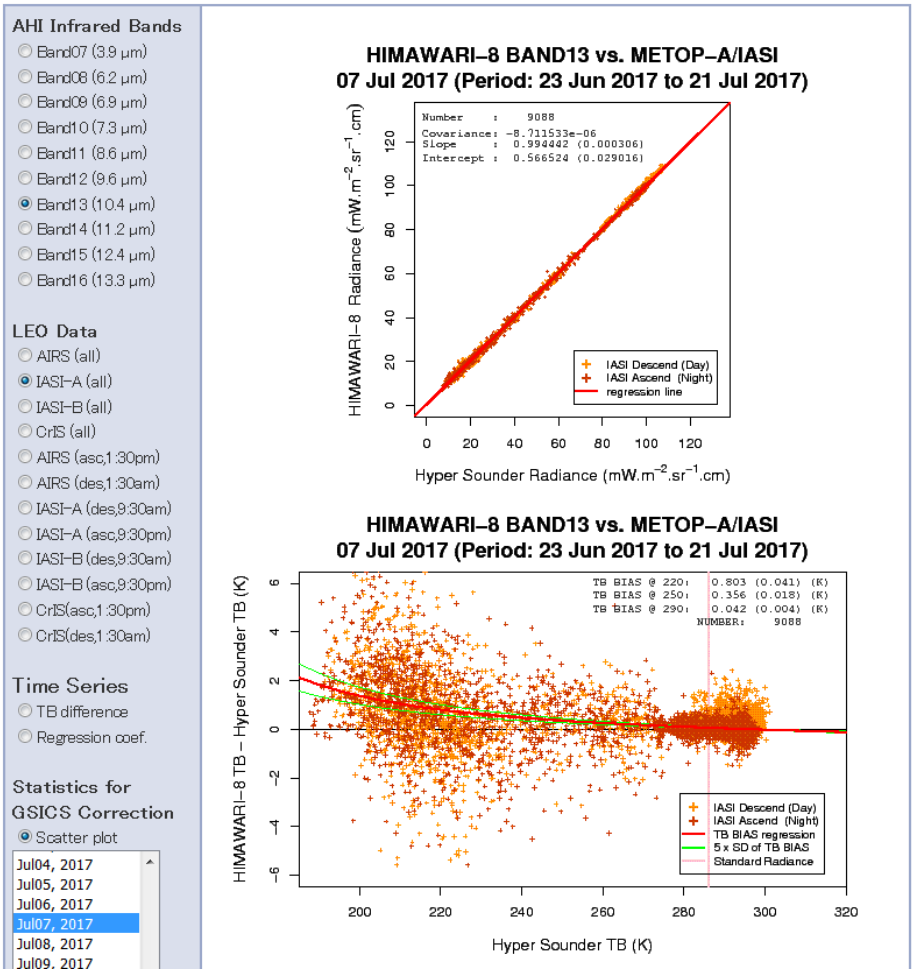

Figure 9: Example of Himawari-8/AHI scatterplot showing regression of collocated radiances, following legend.

5.b.iv. MTSAT/Himawari-AIRS/IASI Specific

Implemented as 5.b.iii.v0.1, but regressions are performed for the collocation data using only LEO ascending paths, only LEO descending paths and both LEO ascending and descending paths, respectively. Note that only night-time data are used for the regression of short wave infrared channels.

5.a.iv.1. **MTSAT-1R Specific**

An uncertainty $\sigma_i = 1$ is assumed.

5.b.iv.2. **MTSAT-2 Specific**

The scatterplot is a plot of the values of MTSAT-2 disseminated digital count (monitored instrument in y axis) versus the corresponding values of AIRS/IASI radiance (reference instrument in x axis). As for the statistical calculation, 5.b.ii.v0.3 was implemented.

5.b.iv.3. **Himawari-8/-9 Specific**

5.b.ii.v0.3 is implemented for the statistical calculation. An example of the scatterplots of the regression data is shown in Figure 9.

5.c. *Bias Calculation*

5.c.i. Purpose

Inter-calibration biases should be directly comparable for representative scenes and conveniently expressed in units understandable by the users. Because biases can be scene-dependent, they are evaluated here at the standard radiances defined in 5.a.

5.c.ii. General Options

5.c.ii.v0.1. Regression coefficients are applied to estimate expected bias, $\Delta\hat{y}(x_{STD})$, and uncertainty, $\sigma_{\hat{y}}(x_{STD})$, for standard radiances, accounting for correlation between regression coefficients.

Equation 20: $\Delta\hat{y}(x_{STD}) = a + bx_{STD} - y_{STD}$,

noting that $y_{STD} = x_{STD}$ and

Equation 21: $\sigma^2_{\hat{y}}(x_{STD}) = \sigma^2_a + \sigma^2_b x^2_{STD} + 2\,\mathrm{cov}(a,b)x_{STD}$

The results may be expressed in absolute or percentage bias in radiance, or brightness temperature differences.

5.c.iii. Infrared GEO-LEO inter-satellite/inter-sensor Class

5.c.iii.v0.1. Biases and their uncertainties are converted from radiances to brightness temperatures for visualisation purposes.

5.c.iv. MTSAT/Himawari-AIRS/IASI Specific

5.c.iv.1. **MTSAT-1R Specific**

Mean TB differences of MTSAT-1R/JAMI radiances from AIRS/IASI ones are computed associated with the regression results at the reference TBs of 290K, 250K and 220K.

5.c.iv.2. **MTSAT-2 Specific**

Mean TB differences of MTSAT-2/Imager radiances from AIRS/IASI ones are computed associated with the regression results at the reference TBs of the standard radiance, 290K, 250K and 220K.

5.c.iv.3. **Himawari-8/-9 Specific**

Mean TB differences of AHI radiances from AIRS/IASI ones are computed associated with the regression results at the reference TBs of the standard radiance, 290K, 250K and 220K.

5.d. *Consistency Test*

5.d.i. Purpose

The most recent results are tested for statistical consistency with the previous time series of results. Users should be alerted to any sudden changes in the calibration of the instruments, allowing them to investigate potential causes and *reset trend* statistics calculated in 5.e. The consistency test may be performed in terms of regression coefficients or biases.

5.d.ii. General Options

5.d.ii.v0.1. The biases calculated for standard radiances from the most recent collocations are compared to the statistics of the biases' trends calculated in 5.e from previous results. If the most recent result falls outside the 3-σ (99.7%) confidence limits estimated from the trend statistics, an alert should be raised. This alert should trigger the Principle Investigator to check the cause of the change and reset the trends by issuing a *trend reset*.

Equation 22: $$\left| \frac{y_i - \hat{y}_i(x_i)}{\sigma_{\hat{y}(x_i)}} \right| \geq Gaussian(=3)$$

5.d.ii.v0.2. The regression coefficients calculated from the most recent collocations are compared to the statistics of the trends calculated from previous regression coefficients. If the most recent result falls outside the 3-σ (99.7%) confidence limits estimated from the trend statistics, an alert should be raised. This has not been implemented yet, due to concerns about correlation between regression coefficients.

5.d.iii. Infrared GEO-LEO inter-satellite/inter-sensor Class

5.d.iii.v0.1. Implement 5.d.ii.v0.1 as above.

5.d.iv. MTSAT/Himawari-AIRS/IASI Specific

5.d.iv.1. **MTSAT-1R/-2 Specific**

Not yet implemented.

5.d.iv.2. **Himawari-8/-9 Specific**

Not yet implemented.

5.e. *Trend Calculation*

5.e.i. Purpose

It is important to establish whether an instrument's calibration is changing slowly with time. It is possible to establish this from a time-series of inter-comparisons by calculating a trend line using a linear regression with date as the independent variable. Only the portion of the time series since the most recent *trend reset* is analysed, to allow for step changes in the instruments' calibration.

5.e.ii. General Options

5.e.ii.v0.1. The time series of biases evaluated at standard radiances can be regressed against the time (date) as the independent variable. The linear regression can be weighted by the calculated uncertainty on each bias. The regression coefficients including uncertainties (and their covariances) are calculated by the least squares method described in 5.b.ii.v0.2. In this case, the variables, x_i and y_i are time series of Julian dates and radiance biases estimated in 0 for each orbit since the most recent *trend reset*, respectively.

5.e.ii.v0.2. It is also possible to perform the trend calculation using the regression coefficients as dependent variables. However, their covariance should also be accounted for and has not been implemented yet.

5.e.iii. Infrared GEO-LEO inter-satellite/inter-sensor Class

5.e.iii.v0.1. Implement 5.e.ii.v0.1 as above.

5.e.iv. MTSAT/Himawari-AIRS/IASI Specific

Not yet implemented. However, time series charts of TB differences between GEO and LEO described in 5.f are updated every day. This monitor shows the trend.

5.f. *Generate Plots for GSICS Bias Monitoring*

5.f.i. Purpose

The results should be reported quantifying the magnitude of relative biases by inter-calibration. This should allow users to monitor changes in instrument calibration.

5.f.ii. General Options

5.f.ii.v0.1. Plots and tables of relative biases and uncertainties for standard radiances should be produced. These may show the evolution of the biases and their dependence on geophysical variables. These all results should be uploaded to the GSICS Data and Products server, and made available from each agency's appropriate inter-calibration webpage.

5.f.iii. Infrared GEO-LEO inter-satellite/inter-sensor Class

5.f.iii.v0.1. Plots should be regularly updated showing the relative brightness temperature biases for the standard radiances in each channel as time series with uncertainties. The trend line and monthly mean biases (and their uncertainties) should be calculated from these time series, following the example in Figure 10. This allows the most recent result to be tested for consistency with the series of previous results. If significant differences are found operators should be alerted, giving them the opportunity to investigate further.

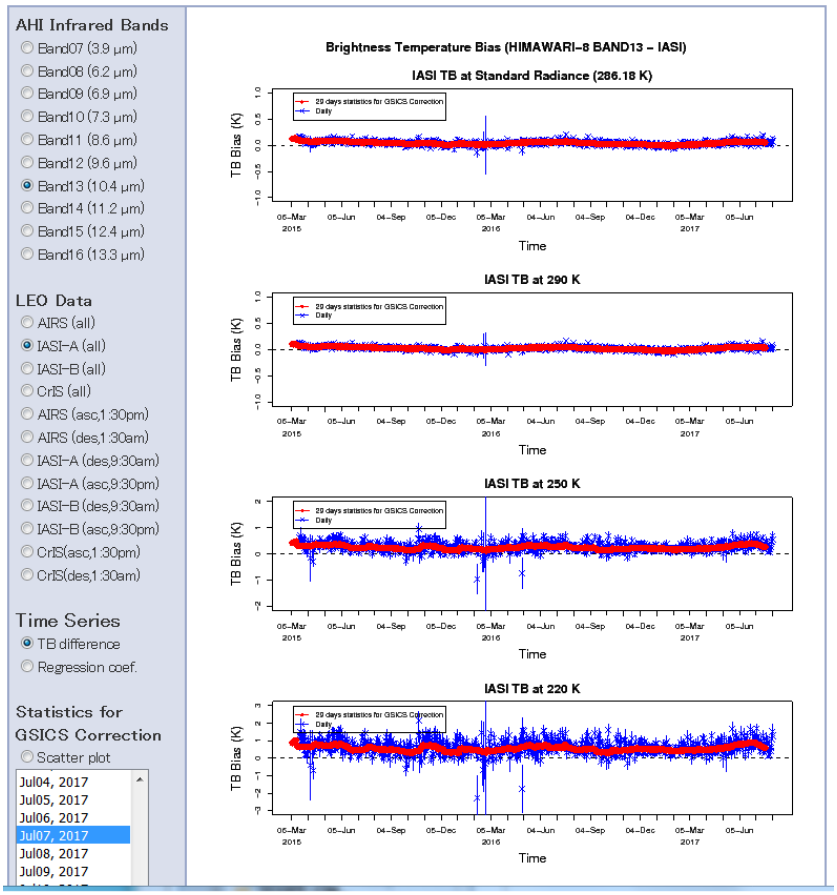

Figure 10: Example of time series plot showing relative bias of Himawari-8/AHI Band 13 (10.4 μm) and Metop-A/IASI at reference radiance following inset legend.

5.f.iv. MTSAT/Himawari-AIRS/IASI Specific

5.f.iv.1. MTSAT-1R/-2 Specific

Time series plots showing TB difference between monitored instrument and reference instrument had been monitored routinely. The results are available on the following JMA website (last access on 10 August 2017):

- MTSAT-1R: http://www.data.jma.go.jp/mscweb/data/monitoring/gsics/ir/gsir_mt1r.html
- MTSAT-2: http://www.data.jma.go.jp/mscweb/data/monitoring/gsics/ir/gsir_mt2.html

5.f.iv.2. Himawari-8/-9 Specific

Time series plots showing TB difference between monitored instrument and reference instrument are monitored routinely. The results are available on the JMA website (last access on 10 August 2017):
http://www.data.jma.go.jp/mscweb/data/monitoring/gsics/ir/monit_geoleoir.html.

6. **GSICS Correction**

This final step of the algorithm is to calculate the GSICS Correction, allowing the calibration of one instrument's observed data to be modified to become consistent with that of the reference instrument. The form of the GSICS Correction will be defined offline and can be instrument specific. However, application of the correction relies on the *Correction Coefficients* supplied by the inter-comparisons performed in the previous steps of the algorithm from the *Analysis Data*.

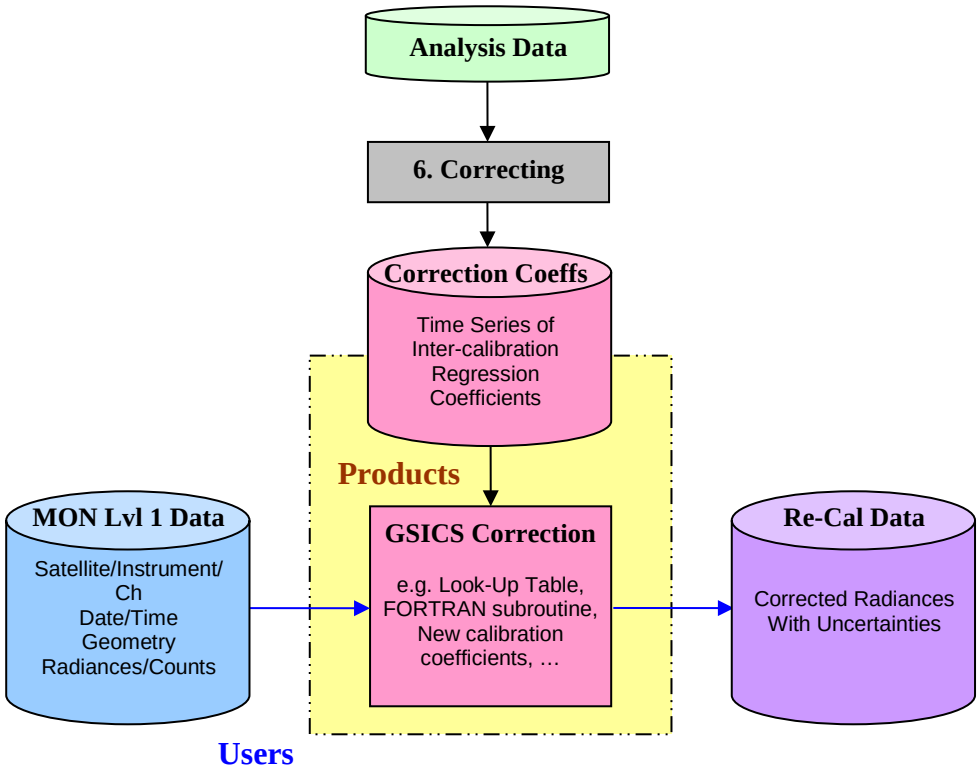

Figure 11: Step 6 of Generic Data Flow, showing inputs and outputs, and illustrating schematically how the correction could be applied by users.

6.a. *Define Smoothing Period (Offline)*

6.a.i. Purpose

It is possible to combine data from a time series of inter-comparison results to reduce the random component of the uncertainty on the final GSICS Correction. However, this requires us to define representative periods over which the results can be smoothed without introducing bias due to calibration drifts during the smoothing period. This period can be defined by comparing the observed rate of change of inter-comparison results with a pre-determined threshold, based on the required or achievable accuracy. In general, this definition is performed offline as it requires an in-depth analysis of the instruments' relative biases and consideration of likely explanatory mechanisms. However, it could also be fine-tuned in near real-time. The following describes the general approaches that should be implemented.

6.a.ii. General Options

6.a.ii.v0.1. In 5.e.ii.v0.1, time series of radiance biases are regressed against date as the independent variable. This yields an estimate of the rate of change of bias with time, $\frac{d\Delta\hat{y}_{REF}}{dt}$, which can be compared to the threshold Δy_{max} to determine the smoothing period, τ_s:

Equation 23: $\tau_s = \Delta y_{\max}\left(\frac{d\Delta\hat{y}_{REF}}{dt}\right)^{-1}$

6.a.ii.v0.2. This component may not be necessary if the time series is interpolated or extrapolated to calculate the GSICS Correction for a particular observation. This would require the regression coefficients to be combined in a time series as suggested in 5.e.ii.v0.2.

6.a.iii. Infrared GEO-LEO inter-satellite/inter-sensor Class

6.a.iii.v0.1. Implement 6.a.ii.v0.1 as above.

6.a.iv. MTSAT/Himawari-AIRS/IASI Specific

6.a.iv.1. MTSAT-1R Specific

The smoothing period is one month. This is only for monthly statistics.

6.a.iv.2. MTSAT-2 Specific

The smoothing periods are 15 days and 29 days for the Near Real Time Correction and Re-Analysis Correction, respectively.

6.a.iv.3. Himawari-8/-9 Specific

The smoothing periods are 15 days and 29 days for the Near Real Time Correction and Re-Analysis Correction, respectively.

6.b. *Calculate Coefficients for GSICS Near-Real-Time Correction*

6.b.i. Purpose

In order to reduce the random component of the uncertainty on the GSICS Correction, it is necessary to combine data from a time series of inter-comparison. The regression process described in 5.b is repeated using all the collocated radiances obtained over the smoothing period defined in 6.a. The resulting regression coefficients (and uncertainties) provide the *Correction Coefficients* used as input to the GSICS Correction. These regression coefficients are then used to evaluate the *Standard Bias* (also with uncertainties) at a set of *Standard Radiances*. The correction coefficients and standard biases are supplied in a netCDF format, which is defined at http://gsics.atmos.umd.edu/bin/view/Development/NetcdfConvention and http://gsics.atmos.umd.edu/bin/view/Development/FilenameConvention (last access on 10 August 2017).

Near Real Time Correction is intended for real-time applications such as data assimilation in operational numerical weather prediction systems and satellite derived level-2 products.

6.b.ii. General Options

6.b.ii.v0.1. The rolling average of the time series of regression coefficients is calculated using a rectangular box-car window with a certain width (e.g. 30 days). The regression coefficients are first transformed to correspond to datasets of centered radiances, after subtracting the standard radiances. This reduces the correlation between the regression coefficients and allows linear averaging.

6.b.ii.v0.2. All the collocation data within the smoothing period is combined and the regression of 5.b repeated on the aggregate dataset. This approach ensures all data is used optimally, with appropriate weighting according to its estimated uncertainty. This is the recommended approach in general for GSICS.

6.b.ii.v0.3. Alternatively, the statistical trends of the time series of regression coefficients suggested in 5.e.ii.v0.2 could be extended – after transforming the dataset to account for the finite covariance between the coefficients. This may be achieved by future developments using Kalman Filtering or EOF-based approaches.

6.b.iii. Infrared GEO-LEO inter-satellite/inter-sensor Class

6.b.iii.v0.1. Implement as 6.b.ii.v0.2. Collocation data for both LEO ascending and descending paths are used for the generation of netCDF files. Note that only night-time data are used for short wave infrared channels.

6.b.iv. MTSAT/Himawari-AIRS/IASI Specific

6.b.iv.1. MTSAT-1R Specific

Not yet implemented.

6.b.iv.2. MTSAT-2 Specific

Implement as 6.b.iii.v0.1, using a smoothing period *t*-14d to *t*-0 (where *t* is the current date).

6.b.iv.3. Himawari-8/-9 Specific

Implement as 6.b.iii.v0.1, using a smoothing period *t*-14d to *t*-0 (where *t* is the current date).

6.c. *Calculate Coefficients for GSICS Re-Analysis Correction*

6.c.i. Purpose

In order to reduce the random component of the uncertainty on the GSICS Correction, it is necessary to combine data from a time series of inter-comparison. The regression process described in 5.b is repeated using all the collocated radiances obtained over the smoothing period defined in 6.a. The resulting regression coefficients (and uncertainties) provide the *Correction Coefficients* used as input to the GSICS Correction. These regression coefficients are then used to evaluate the *Standard Bias* (also with uncertainties) at a set of *Standard Radiances*. The correction coefficients and standard biases are supplied in a netCDF format, which is defined at http://gsics.atmos.umd.edu/bin/view/Development/NetcdfConvention and http://gsics.atmos.umd.edu/bin/view/Development/FilenameConvention (last access on 10 August 2017).

Re-Analysis Correction is intended for reprocessing type analysis, as it has a longer smoothing period than *Near Real Time Correction* to allow more smoothing of the results by combining more collocations (i.e., smoothing period is defined to be symmetric about the validity date of the GSICS Correction coefficients). This requires us to perform this step after a correspond delay of at least half the smoothing period after the validity date.

6.c.ii. General Options

6.c.ii.v0.1. As 6.b.ii.v0.1.

6.c.ii.v0.2. As 6.b.ii.v0.2.

6.c.ii.v0.3. As 6.b.ii.v0.3.

6.c.iii. Infrared GEO-LEO inter-satellite/inter-sensor Class

6.c.iii.v0.1. Implement as 6.b.iii.v0.1.

6.c.iv. MTSAT/Himawari-AIRS/IASI Specific

6.c.iv.1. MTSAT-1R Specific

Not yet implemented.

6.c.iv.2. MTSAT-2 Specific

Implement as 6.c.iii.v0.1, using a smoothing period *t*-14d to *t*+14 (where *t* is the validity date).

6.c.iv.3. Himawari-8/-9 Specific

Implement as 6.c.iii.v0.1, using a smoothing period *t*-14d to *t*+14 (where *t* is the validity date).

6.d. *Calculate Inter-Calibration Coefficients*

6.d.i. Purpose

This component aims to produce revised sets of calibration coefficients for one instrument following its inter-calibration against a reference instrument using the *Analysis Data* provided by Step 4. These would allow users to recalibrate data from the monitored instrument to be consistent with the reference instrument.

6.d.ii. General Options

6.d.ii.v0.1. The regression coefficients provided as the *Analysis Data* output from Step 4 are transformed to generate new *correction coefficients* (together with estimates of their uncertainties as full covariances). These can then be used to convert the observations of the monitored instrument into radiances consistent with the GSICS reference standard.

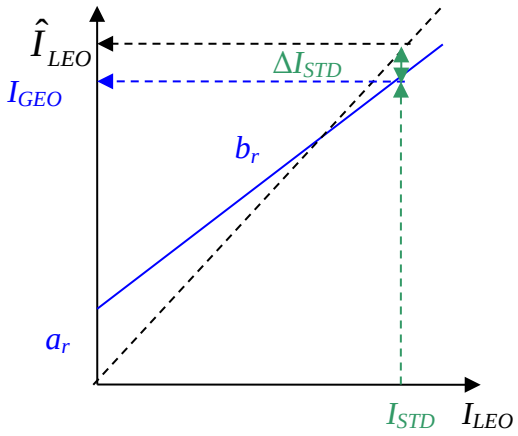

Figure 12: Relationship between radiances observed by geostationary instrument, I_{GEO} and those observed by reference instrument in low Earth orbit, I_{LEO}, showing relative bias for standard radiance, I_{STD}.

6.d.iii. Infrared GEO-LEO inter-satellite/inter-sensor Class

6.d.iii.v0.1. The regression of the aggregated collocated radiances in 6.b.ii.v0.2 and 6.c.ii.v0.2 yields estimates of the coefficients, a_r and b_r, required to convert GEO radiances, I_{GEO}, to the reference LEO radiances, I_{LEO}:

Equation 24: $I_{GEO} = a_r + b_r I_{LEO}$

This relationship can be inverted to apply the regression coefficients, a_r and b_r, to convert GEO radiances, I_{GEO}, into radiances consistent with the LEO reference instrument, $\hat{I}_{LEO}$,

Equation 25: $\hat{I}_{LEO} = -\frac{a_r}{b_r} + \frac{1}{b_r} I_{GEO}$,

together with the estimated uncertainty:

Equation 26: $\sigma^2_{\hat{I}_{LEO}} = \left(\frac{\sigma_{a_r}}{b_r}\right)^2 + \left[(I_{GEO} - a_r)\sigma_{b_r}\right]^2 - 2\frac{(I_{GEO} - a_r)}{b_r}\sigma_{a_r b_r}$,

6.d.iv. MTSAT/Himawari-AIRS/IASI Specific

6.d.iv.1. **MTSAT-1R Specific**

Implemented as 6.d.iii.v0.1.

6.d.iv.2. **MTSAT-2 Specific**

For MTSAT-2/Imager, the disseminated HRIT data contains the calibration look-up table which converts digital count to the brightness temperature. For the users' convenience, our proposal to adopt a regression formula directly converting digital count to corrected radiance for MTSAT's GSICS Correction was approved at the GSICS web meetings.

In this approach, the regression coefficient, *a* and *b*, (and their uncertainties) can be expressed by the following equation. The regression formula converts LEO radiances, I_{LEO}, into GEO digital counts, C_{GEO}:

Equation 27: $C_{GEO} = a + b \times I_{LEO}$

This relationship can be inverted to apply the regression coefficients, *a* and *b*, to convert GEO digital counts, C_{GEO}, into radiances consistent with the LEO reference instrument, $\hat{I}_{LEO}$:

Equation 28: $\hat{I}_{LEO} = a_g + b_g C_{GEO}$, where $a_g = -\frac{a}{b}$ and $b_g = \frac{1}{b}$.

where a_g and b_g are new calibration coefficients (with uncertainties) which convert GEO counts, C_{GEO}, into radiances consistent with the LEO reference instrument, $\hat{I}_{LEO}$, together with the estimated uncertainty:

Equation 29: $\sigma^2_{\hat{I}_{LEO}} = \left(\frac{\sigma_a}{b}\right)^2 + \left[(C_{GEO} - a)\sigma_b\right]^2 - 2\frac{(C_{GEO} - a)}{b}\sigma_{ab}$,

6.d.iv.3. **Himawari-8/-9 Specific**

Implemented as 6.d.iii.v0.1.

References

Clough, S. A., and M. J. Iacono, 1995: Line-by-line calculations of atmospheric fluxes and cooling rates II: Application to carbon dioxide, ozone, methane, nitrous oxide, and the halocarbons. *J. Geophys. Res.*, **100**. 16519-16535.

Gunshor, M.M., T.J. Schmit, W.P. Menzel, and D.C. Tobin, 2009: Intercalibration of Broadband Geostationary Imagers Using AIRS, *Journal of Atmospheric and Oceanic Technology*, vol. **26**, 746-758.

Hewison, T.J., 2009: Quantifying the Impact of Scene Variability on Inter-Calibration, *GSICS Quarterly*, Vol. **3**, No. 2, 2009.

Minnis, P., A. V. Gambheer, and D. R. Doelling, 2004: Azimuthal anisotropy of longwave and infrared window radiances from CERES TRMM and Terra data. *J. Geophys. Res.*, **109**, D08202, doi:10.1029/2003JD004471.

Press, W.H., S.Teukolksy, W.T.Vetterling and B.Flannery, 1995: Numerical recipes: the art of scientific computing, Second edition, Cambridge University Press.

Rothman et al., 2003: The HITRAN molecular spectroscopic database: edition of 2000 including updates through 2001, *Journal of Quantitative Spectroscopy and Radiative Transfer*, vol. **82**, 5-44.

Tahara, Y., 2008a: Central Wavelengths and Wavenumbers and Sensor Planck Functions of the GMS and MTSAT Infrared Channels, *Meteorological Satellite Center Technical Note*, No. **50**, 51-59 (in Japanese).

Tahara, Y., 2008b: New Approach to Intercalibration Using High Spectral Resolution Sounder, *Meteorological Satellite Center Technical Note*, No. **50**, 1-14.

Tahara, Y. and K. Kato, 2009: New Spectral Compensation Method for Intercalibration Using High Spectral Resolution Sounder, *Meteorological Satellite Center Technical Note*, No. **52**, 1-37.

Tobin, D. C., H. E. Revercomb, C. C. Moeller, and T. Pagano, 2006: Use of Atmospheric Infrared Sounder high-spectral resolution spectra to assess the calibration of Moderate re solution Imaging Spectroradiometer on EOS Aqua, *J. Geophys. Res.*, **111**, D09S05, doi:10.1029/2005JD006095.

Wu, X., 2009: GSICS GOES-AIRS Inter-Calibration Algorithm at NOAA GPRC, Draft version dated January 5, 2009.

APPENDIX

Sensor Planck Functions for AHIs on the Himawari-8 and -9

The Planck function and sensor spectral response functions are used to compute brightness temperature [K] from radiance [mW/m^2/sr/cm^{-1}] and vice-versa. In general, approximation equations called *sensor Planck functions*, which are generated for AHI infrared bands, are used to facilitate computation. *Central wavenumbers* and *band correction coefficients* needed for *sensor Planck functions* of Himawari-8 and -9 AHI infrared bands are shown in Tables 2 and 3.

Brightness temperature to radiance

$$B_i(T_b) = \frac{2\,h\,c^2\,\nu_i^3}{\exp\{h\,c\,\nu_i\,/\,k\,(a_{1i} + a_{2i}\,T_b) - 1\}}$$

where B_i: sensor Planck function of band i
T_b: brightness temperature
ν_i: central wavenumber of band i
a_{1i}, a_{2i}: band correction coefficients of band i
h: Planck constant
k: Boltzmann constant
c: speed of light

Radiance to brightness temperature

$$T_b = b_{1i} + b_{2i}\,T_e + b_{3i}\,T_e^2,$$

$$T_e(B_i) = \frac{\frac{hc}{k}\,\nu_i}{ln(\frac{2\,h\,c^2\,\nu_i^3}{B_i} + 1)}.$$

where T_b: the Planck temperature of band i
T_e: effective temperature
B_i: spectral radiance
b_{1i}, b_{2i}, b_{3i}: band correction coefficients of band i

Table 2: Central wavenumber and band correction coefficients for Himawari-8/AHI Sensor Planck Functions.

AHI band	Wavenumber	Band correction coefficients				
	ν (cm^{-1})	a1	a2	b1	b2	b3
Band 7 (3.9 μm)	2575.767	0.464673802	0.999341618	-0.479757	1.000766	-1.860569e-07
Band 8 (6.2 μm)	1609.241	1.646844799	0.996401237	-1.662616	1.003694	-1.732716e-07
Band 9 (6.9 μm)	1442.079	0.30813537	0.999259063	-0.3357036	1.000974	-4.847962e-07
Band 10 (7.3 μm)	1361.387	0.057369468	0.999854346	-0.06306013	1.000195	-1.069833e-07
Band 11 (8.6 μm)	1164.443	0.135127541	0.999615566	-0.1605105	1.000589	-4.019762e-07
Band 12 (9.6 μm)	1038.108	0.093630424	0.999703302	-0.1143507	1.000473	-3.67168e-07
Band 13 (10.4 μm)	961.333	0.089654915	0.999700114	-0.1192115	1.000539	-4.680314e-07
Band 14 (11.2 μm)	890.741	0.180093131	0.999356159	-0.2530423	1.001233	-1.153788e-06
Band 15 (12.4 μm)	809.242	0.243907194	0.999046134	-0.3766459	1.002025	-2.096994e-06
Band 16 (13.3 μm)	753.369	0.062356354	0.999737103	-0.09773197	1.000564	-6.266746e-07

Table 3: Central wavenumber and band correction coefficients for Himawari-9/AHI Sensor Planck Functions.

AHI band	Wavenumber	Band correction coefficients				
	ν (cm^{-1})	a1	a2	b1	b2	b3
Band 7 (3.9 μm)	2613.607	0.4517128	0.9993711	-0.462818	1.000709	-1.3764480E-07
Band 8 (6.2 μm)	1607.897	1.631702	0.9964356	-1.643762	1.003627	-1.0159740E-07
Band 9 (6.9 μm)	1438.94	0.2696262	0.9993508	-0.2934427	1.000851	-4.1930330E-07
Band 10 (7.3 μm)	1361.95	0.05705145	0.9998552	-0.06265289	1.000194	-1.0530290E-07
Band 11 (8.6 μm)	1164.303	0.131854	0.9996248	-0.1567172	1.000576	-3.9375000E-07
Band 12 (9.6 μm)	1039.153	0.09237552	0.9997075	-0.1127442	1.000466	-3.6094580E-07
Band 13 (10.4 μm)	961.334	0.09140126	0.9996943	-0.1214194	1.000548	-4.7535350E-07
Band 14 (11.2 μm)	893.216	0.1767254	0.9993697	-0.2478741	1.001205	-1.1253390E-06
Band 15 (12.4 μm)	810.25	0.241578	0.9990565	-0.3724054	1.001999	-2.0668740E-06
Band 16 (13.3 μm)	751.674	0.062358	0.9997365	-0.0979252	1.000566	-6.3006570E-07